Çukurova Üniversitesi Mühendislik Mimarlık Fakültesi Dergisi, 35(1), ss. 127-138, Mart 2020
Çukurova University Journal of the Faculty of Engineering and Architecture, 35(1), pp. 127-138, March 2020

Fabrication and Characterization of CuO Nanostructures: Applications in Electrocatalytic Hydrogen Production

Evrim BARAN AYDIN[*1]

[1]*Department of Mechanical Engineering, Faculty of Engineering and Architecture, University of Kilis 7 Aralık, Kilis*

Geliş tarihi: 14.11.2019 Kabul tarihi: 15.05.2020

Abstract

Hydrogen which is a renewable and sustainable form of energy to replace fossil fuels has been has been attracted great interest because of clean emission and high conversion efficiencies. To make water electrolyzer more profitable and economical, the selection of electrodes having low overpotentials, low-cost and stable with well electrocatalytic activity is required. In this study, CuO nanostructures were fabricated by chemical techniques. The morphologies and structures of CuO nanostructures were studied in detail by FE-SEM, BET, and XRD. Three different morphologies of CuO (Nanorod, nanoflake and nano-flower nanostructures) were synthesized. The contact angle measurements were carried out to state the surface properties of the synthesized materials. The cathodic polarization, open circuit potential-time measurements, impedance measurements and Mott-Schottky analysis were carried out in 1M KOH solution to determine the electrocatalytic performance of electrodes in hydrogen formation reaction. Besides, energy consumption efficiencies of electrodes for alkaline electrolysis were investigated.

Keywords: CuO, Nanostructures, Hydrogen evolution, Energy requirement

CuO Nanoyapıların Karakterizasyonu ve Üretimi: Elektrokatatlitik Hidrojen Üretimindeki Uygulamaları

Öz

Yenilenebilir ve sürdürülebilir bir enerji şekli olarak fosil yakıtların yerini alabilecek başlıca enerji kaynaklarından biri olan hidrojen, temiz emisyon ve yüksek dönüşüm verimliliği nedeniyle artan bir ilgi görmektedir. Suyun elektrolizi ile H_2 üretimini daha verimli ve ekonomik hale getirmek için, elektrotların aşırı gerilimlerinin azaltılması ve aynı zamanda, iyi bir elektrokatalitik etkinliğe sahip ucuz ve kararlı elektrotların seçilmesini gerektirir. Bu çalışmada, CuO nanoyapılar, kimyasal teknikle sentezlenmiştir. CuO nanoyapıların morfolojileri ve yapıları, FE-SEM, BET ve XRD ile ayrıntılı olarak karakterize edilmiştir. Üç farklı morfolojiye sahip CuO nanoyapılar (Nanorod, nanoflake ve nano-çiçek) elde edilmiştir Elde edilen malzeme yüzeylerinin ıslanma davranışını belirlemek için temas açısı ölçümleri kullanılmıştır. Elektrotların hidrojen oluşum reaksiyonundaki elektrokatalitik etkinliği hakkında bilgi edinmek amacıyla katodik polarizasyon, açık devre-süre ölçümleri, impedans ölçümleri ve Mott-Schottky analizi 1M KOH çözeltisinde gerçekleştirilmiştir. Ayrıca, alkalin elektroliz için elektrotların enerji tüketim verimlilikleri incelenmiştir.

Anahtar kelimeler: CuO, Nanoyapılar, Hidrojen evrimi, Enerji ihtiyacı

[*]Sorumlu yazar (Corresponding author): E. Baran AYDIN, *evrimbaran@kilis.edu.tr*

1. INTRODUCTION

The energy requirement in the world is increasing rapidly. The supply of energy requirements without polluting the environment forms the basis of the study subjects. In this context, it is accepted that the most advanced technology is the hydrogen energy system. Hydrogen energy does not threaten human and environmental health. Hydrogen can be obtained from fossil fuels such as coal and natural gas, as well as from water and biomass. An ideal energy fuel should be easily and safely transported anywhere, the energy loss during transport should be little or no, it should be stored, inexhaustible, safe, very light, carbon-free and economical. In this context, hydrogen can be considered as a clean energy source that can replace fossil fuels with zero carbon emission, recyclability and high energy capacity [1,2]. Techniques such as electrolysis, photocatalysis and thermolysis are commonly used for hydrogen production. Photoelectrochemical cells are being investigated extensively not only because they enable the electrolysis of water by utilizing solar energy, but also by separating the hydrogen formation reaction (HER) and oxygen formation reaction (OER) mechanisms, thereby enabling kinetic investigations of each half cell reaction. Various semiconductors have been promising for the production of hydrogen by photoelectrochemical separation of water due to their long-term chemical stability and high electron efficiency [3-5]. Generally, n-type semiconductors such as TiO_2 [5], WO_3 [6], Fe_2O_3 [7], $BiVO_4$ [8] and Ag_3PO_4 [9] are more positive than the valence band region H_2O/O_2 redox pair. They can be used as photoanodes for the reaction. On the other hand, p-type semiconductors whose conductor band edge is more positive than H_2O/H_2 potential can be used as photocathodes for HER [10]. For example, p-$GaInP_2$ [11], p-InP [12], p-WSe [13], p-Si [14], p-CdS [15], and p-type copper oxides have been investigated as possible candidates for photocathode in water electrolysis. Among these p-type semiconductors, cupric oxides (Cu_2O and CuO) are great interest due to its wide absorption band in the visible area, high availability in the earth's crust, easy to prepare, low cost and low environmental toxicity. The formation of these oxides depends on the conditions under which oxidation occurs. Metallic copper, CuO and Cu_2O have different crystal structures. The easy reduction of CuO to Cu_2O and the high stability of Cu_2O are because that the oxygen bond energy of Cu_2O is much higher than that of CuO. However, CuO has higher solar absorption than Cu_2O because it has a smaller bandgap of 1.5 eV [16].

Copper is used in solar panels, magnetic storage, electronic devices, catalyst and gas sensors due to its unique thermal, magnetic, optical and catalytic properties. It is of particular importance in the electrical/electronics industry, especially because of its low cost. The interest in nano-scale structures is increasing day by day with the expansion of the usage areas. Studies show that metal nanomaterials have superior electronic, magnetic, optical, chemical and catalytic properties depending on their size, shape, surface components and atomic arrangement on the surface. CuO nanostructures such as thin-film nanoparticles, nanowires, nanorods, nanoscreens, nanomembranes and microflores can be synthesized using direct thermal oxidation of copper plates and hydrothermal methods [17]. On the other hand, a very small group succeeded in the synthesis of CuO nanotube using expensive and complex methods based on anodic aluminum oxide membrane template [18], hydrothermal treatment of $Cu(OH)_2$ and direct thermal oxidation of copper. CuO nanostructures are thought to be active in photocatalytic reduction of water.

In the present study, CuO nanostructures were synthesized by the chemical technique. The morphologies and structures of CuO nanostructures were characterized in detail by FE-SEM, BET, and XRD. Cathodic polarization, impedance measurements and Mott-Schottky analysis were carried out in 1M KOH solution to attain information about the electrocatalytic activity of electrodes in hydrogen formation reaction. Also, energy consumption efficiencies of electrodes for alkaline electrolysis were investigated.

2. MATERIALS AND METHODS

2.1. Materials

Copper foils with the thickness of 0.5 mm (99.9% purity) were used at all the experiments. Ammonium persulfate ($(NH_4)_2S_2O_8$, 98%), Sodium hydroxide (NaOH), hydrochloric acid (HCl, 37%), acetone, and ethanol were bought in Merck company. The experiments were performed at 25°C and distilled water were used in the experiments. The analytical grade chemicals without any further purification were used during all the work.

2.2. Synthesis of the CuO Nanostructure

Before the synthesis of CuO nanostructures, the Cu foils with the size of 1.5x1 cm were chemically polished in 3M HCl for 10 min to remove the surface impurities and following, mechanically polished were performed. Finally the foils were degreased by ultrasonic cleaning in acetone, ethanol and distilled water for 10 min, respectively. Then the oxygen stream was used to dry the foils. The pre-cleaned Cu foils were immersed in a solution containing 13 mL of 10 M NaOH, 5 mL of 1 M $(NH_4)_2S_2O_8$, and 48 mL of deionized water for 30, 60 to 180 min. The foils with a layer of $Cu(OH)_2$ nanostructures were then rinsed with ethanol and deionized water and dried in air. To obtain crystalline CuO nanostructures, the heat treatment was performed. The foils were exposed to 150 °C for 1 h to remove the water, and then the temperature was raised to 200 °C, and this process was applied for 2 hours to provide crystallization in air atmosphere.

2.3. Characterization of the CuO Nanostructures

The Zeiss/Supra 55 field emission-scanning electron microscope (FE-SEM) at high vacuum and 10.00 kV EHT was utilized to attain information about surface characterization of the CuO nanostructures. The Rigaku Smart Lab diffractometer (XRD) with Cu Kα radiation employed at 40 kV and 30 mA between 2θ values of 20-80° with a scan rate of 5 ° min^{-1} was used to determine the crystal phases of the samples. The manual optical tensiometer (KSV Attension ThetaLite TL 101) was employed to examine the water contact angle of the surface of the samples, using the sessile drop method. the Vickers hardness of electrodes were measured by Shimadzu HMV-G microhardness tester with a load of 490.3 mN and a dwell time of 7 s.

2.4. Electrochemical Measurements

The electrochemical impedance spectroscopy (EIS) and other electrochemical measurements were benefited from the CHI 604E A.C. electrochemical analyzer. In this measurement, a platinum sheet (with 2 cm^2 surface area) as the counter electrode and Ag/AgCl (3 M KCl) electrode as the reference electrode were utilized.

The EIS measurements were recorded between 100 kHz and 0.01 Hz with the amplitude voltage of a 5 mV at the open circuit potential in 1 M KOH media. The fitting of the results of EIS measurements was performed using the Zview software. The charge carrier density and flat band potential of the electrodes were determined using the Mott–Schottky (MS) approach. The Mott-Schottky measurements were recorded at 10^3 Hz and the range of -0.2 to 0.8 V vs. Ag/AgCl (3 M KCl) in 1 M KOH electrolyte. In the MS measurements, potential step was selected as 10 mV. The current-potential curves were recorded at the potentials from the open circuit potential (OCP) down to -1.8 V. The measurements were carried out after the time necessary to reach a quasi-stationary value (1 h). In this measurement, a scan rate of 5 mV s^{-1} was chosen.

The H_2 evolution measurements of the electrodes were carried out under bias voltages of -1.8, 2.0 and 2.2 V for 30 min in 1M KOH solution in 3 replications. A reverted burette was utilized for the measurements of the evolution H_2 gas amount during the process. The energy efficiency and consumption measurements of the electrodes were carried out by CHI 660D Potentiostat/Galvanostat in 1M KOH electrolyte at 298 K. In the measurements, the current densities were selected as 25, 50 and 100 mA cm^{-2}. The electrolysis time

of 30 min was applied for the energy efficiency and consumption measurements.

3. RESULTS AND DISCUSSION

3.1. Structural Properties of CuO Nanomaterials

A rapid oxidation of the copper surface by the presence of ammonium persulfate results in the formation of copper hydroxide ($Cu(OH)_2$) on the surface. Also, Sodium hydroxide can oxidize the copper surface even though it lasts longer [19]. The released Cu^{2+} cations subsequently react with the hydroxide anions in the solution to create $Cu(OH)_2$ on the substrate. The light blue $Cu(OH)_2$ layer appeared on the surface of Cu foil is slowly turned into the CuO by heat treatment. The overall chemical equation is summarized in Equations 1 and 2 [20,21];

$$Cu + S_2O_8^{-2} + 2OH^- \longrightarrow Cu(OH)_2 + 2SO_4^{-2} + 2H_2O \quad (1)$$

$$Cu(OH)_2 \xrightarrow{\Delta} CuO + H_2O \quad (2)$$

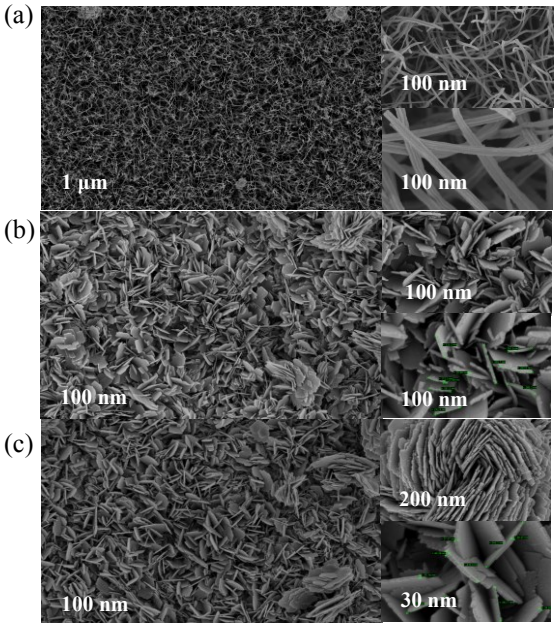

Figure 1. FE-SEM (top and cross section views) of (a) CuO-30 min, (b) CuO-60 min, and (c) CuO-1800 min electrodes

After immersed into the alkaline solution at the 30 min, CuO nanorod array structures are formed on the substrates and exhibit a well uniformity, as shown in Figure 1a. The nanorods having a diameter of about 155-237 nm developed obliquely to form grasslike clusters that overlap and interlace each other. Increasing the reaction time to 60 minutes, the rods totally disappeared and the copper layer surface is only covered by the nanostructure which are composed of interconnected thin flakes, due to a partial dissolution of the center of the rods. As can be seen from Figure 1b, the average nano-flakes corner length and the thickness of the flakes nanostructures were found to be 246.10±79.25 nm and 33.56 nm±5.16, respectively. The stacking the nanoribbons with hydrogen bonding interactions creates the nanorods. The high NaOH concentration leads to weakening of the interlayer hydrogen bond linkages at the sheet edges. this causes stresses in the layers. for this reason, the ribbons were rolled to decrease the stresses, yielding the ultimate tubular structure. When the reaction time was sustained to 1800 min, the structure of nanoflakes CuO formed on the substrate increase in the surface and fower-like morphological structures are formed in certain regions. As shown in Figure 1c, the thickness of the nano-flakes and the average nano-flakes corner length were determined to be 33.56 nm±5.16 and 418.32±79.25 nm, respectively.

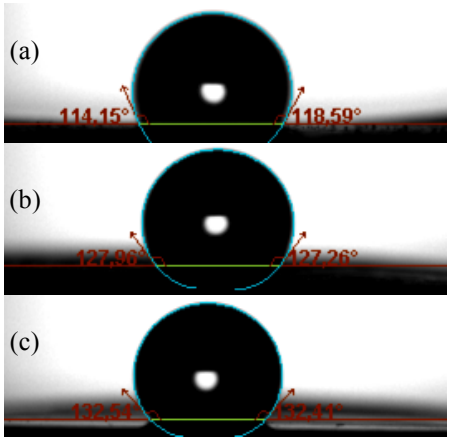

Figure 2. Water contact angles images of (a) CuO-30 min, (b) CuO-60 min, (c) and (c) CuO-1800 min electrodes

Figure 2 shows the contact angle measurement results of CuO nanostructures. The contact angles of the nanorod, nanoplate (nanoflakes) and nano-flower-like CuO structures with water were determined as 116.4°, 127.6° and 132.5°, respectively. The results show that the surface exhibits hydrophobic behavior and that the surface goes towards superhydrophobicity depending on the surface morphology. Superhydrophobic surfaces generally have contact angle values of 150° or greater. Superhydrophobic surfaces exhibit properties such as low energy surface and high surface roughness. The changes such as surface chemical composition, morphology, and surface roughness formed on the surface of CuO materials can directly influence the wetting behavior. Wetting behavior of micro- and nanostructured CuO layer surfaces is closely related to morphological factors such as curtain, height and shape [22].

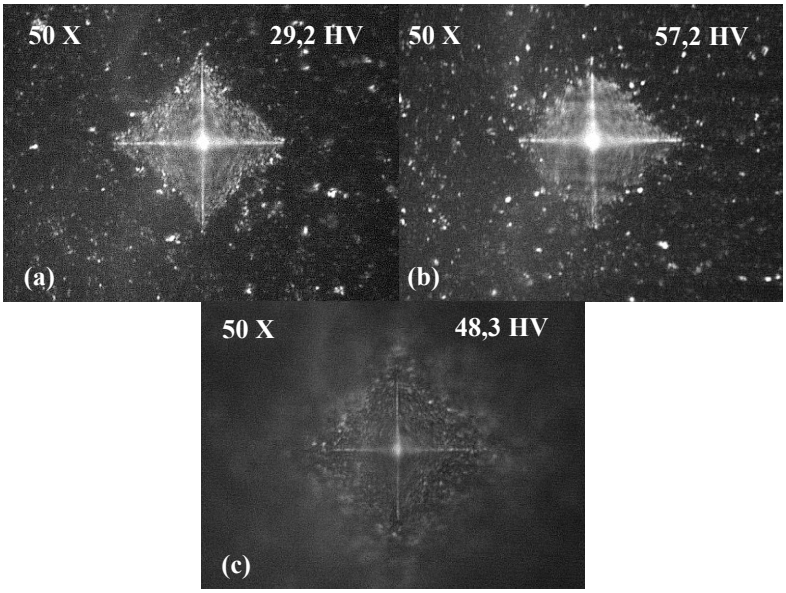

Figure 3. Microhardness results under indentation loads of 490.3 mN for (a) CuO-30 min, (b) CuO-60 min, (c) and (c) CuO-1800 min electrodes

Microhardness measurement results of CuO nanostructures synthesized chemically at different times are presented in Figure 3. Microhardness results in Vickers for CuO-30 min, CuO-60 min, v CuO-1800 min electrodes were 29, 48 and 57 HV, respectively. The results showed that the surface morphology changed with increasing time caused small changes on the hardness and the increase in the hardness value partly due to the decreased surface stress of the nano-flower morphology produced at 1800 min.

Figure 4 shows the XRD results of heat-treated and without heat-treated Cu/CuO nanostructures after immersion in $NaOH/(NH_4)_2S_2O_8$ aqueous solution for 30-1800 minutes. In all XRD results, three peaks with 2θ value of 43°, 51° and 75° corresponding to the planes of Cu (111), (200) and (220) were observed (JCPDS file No. 04–0836) [23]. As seen from the XRD result of the CuO-30 min electrode without heat treatment, the diffraction peaks having values of 2θ to about 24°, 34°, 36°, 38°, 40° and 53° can be indexed the planes of the orthorhombic $Cu(OH)_2$ planes of (002), (111), (022), (130) ve (132) (JCPDS file no. 80-0656) [24]. When XRD results of heat treated CuO-30, CuO-60 and CuO-1800 electrodes were examined, orthorhombic $Cu(OH)_2$ peaks disappeared, and the CuO peaks in 2θ values at 35.5° ve 38.8° corresponding to (002) and (111) planes were formed. (JCPDS file No. 80-1916) [25].

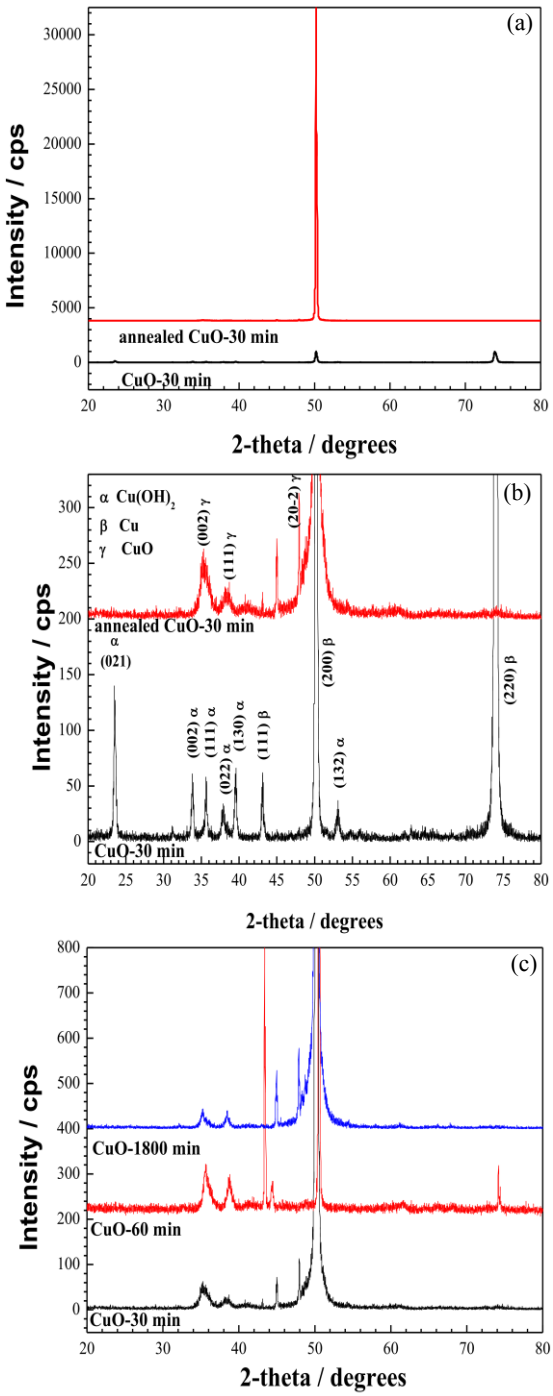

Figure 4. XRD patterns of CuO-30 min without heat, annealed CuO-30 min, CuO-60 min, and CuO-1800 min electrodes

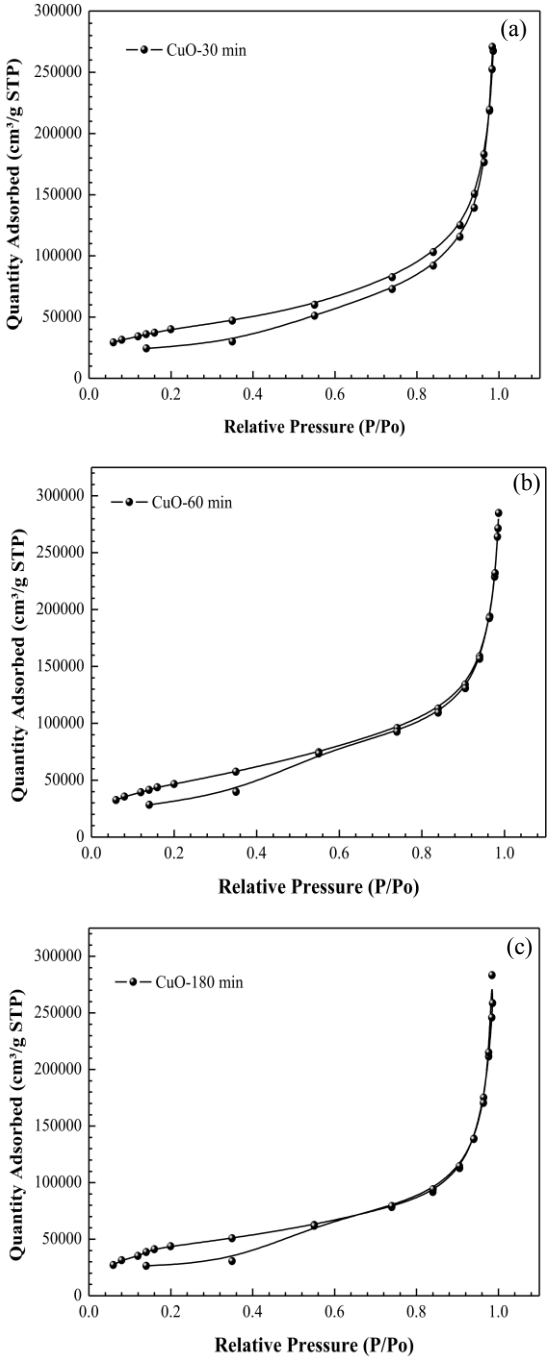

Figure 5. The measurement results according to Brunauer-Emmett-Teller using nitrogen gas for CuO-30 min (a), CuO-60 min (b), and CuO-1800 min (c) electrodes

As can be seen from Figure 5, the BET surface areas of CuO-30 min, CuO-60 min, and CuO-1800 min electrodes were determined as 11.6, 14.6 and 12.1 m^2/g, respectively. The results indicated that the surface area did not change significantly depending on the change in the surface morphology.

3.2. Electrochemical Characterization of CuO Nanostructures

Open circuit potentials (OCP) as a function of time in 1 M KOH electrolyte for CuO-30 min, CuO-60 min and CuO-1800 min electrodes are given in Figure 6. Figure 6 shows that the CuO-30 min electrode has more negative open circuit potential. It indicates that CuO-30 min electrode with more negative potential is more active in hydrogen formation reaction (HER) than other electrodes.

Electrochemical impedance (EIS) results recorded in open circuit potential (OCP) in 1 M KOH electrolyte for CuO-30 min, CuO-60 min and CuO-1800 min electrodes are presented in Figure 7. The charge transfer resistances of CuO-30 min, CuO-60min and CuO-1800 min electrodes from Nyquist curves were determined as 472 Ω cm^2, 639 Ω cm^2 and 1100 Ω cm^2, respectively. When the charge transfer resistors are considered, it is seen that CuO-30 min electrode has lower resistance value. The low resistance value indicates that the nanorod structure acts as free electroactive adsorption zones by increasing the H+ adsorption in the active cathodic regions of the nanorod morphology of CuO-30 min electrode. This event increases HER catalytic activity [26].

Mott-Schottky (M-S) analysis was carried out to investigate the variation in capacitances at the semiconductor-electrolyte interface with the applied voltage. M-S analysis was employed to obtain the flat band potentials (E_{FB}) and the charge carrier densities (N_D) of CuO electrodes.

$$\frac{1}{C^2}=\frac{2}{q\varepsilon\varepsilon_0 N_D}\left[(E-E_{FB})-\frac{k_B T}{q}\right] \quad (3)$$

Where C, ε, ε_0 and q are the capacitance ($F.cm^{-2}$), the relative permittivity of CuO, the vacuum permittivity ($8.854.10^{-12}$ $F.m^{-1}$) and elementary electric charge ($1.602.10^{-19}$ C), respectively. Capacitance C was calculated from the following equation;

$$C=(2\pi fZ'')^{-1} \quad (4)$$

Where f is the frequency (10^3 Hz) and Z'' is the imaginary component of the impedance. As can be seen from Figure 8, the Mott-Schottky plots have a positive slope characteristic with n-type semiconductor behavior [27]. The flat band potentials for CuO-30 min, CuO-60 min and CuO-1800 min electrodes were calculated as 0.03 V, 0.04 V and 0.18 V, respectively. The flat band potential has shifted to a more positive potential with increasing time. This indicates that the bandgap is wider and that much less electrons occur at the semiconductor interface. The CuO-30 min electrode is lower than the flat band potential when compared with other electrodes. The cathodic shift in the flat band potential also provides an easy charge transfer [28].

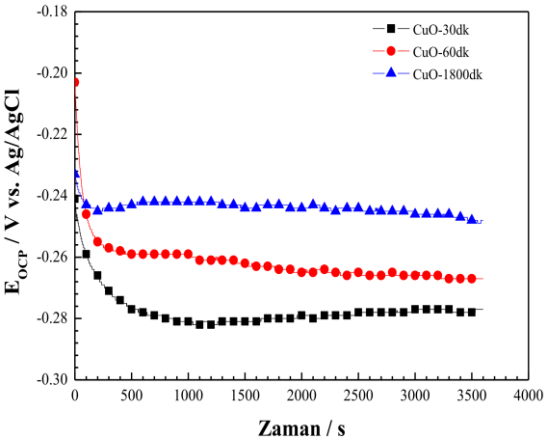

Figure 6. Variation of open circuit potential as a function of time in 1 M KOH electrolyte for CuO-30 min, CuO-60 min, and CuO-1800 min electrodes

Figure 9 shows the cathodic polarization curves recorded for CuO-30 min, CuO-60 min, and CuO-1800 min electrodes at 1 M KOH. As can be

seen, in Figure 9, when the coating time is increased, the open circuit potential shifts to more negative values. At high pH values at the -0.8/-1.2 V potential range, CuO is converted to CuO_2^{-2} oxy- anion ($CuO+H_2O \rightarrow 2H^+ + CuO2^{-2}$) and at high pH CuO_2^{-2} is stable. The current density towards cathodic potential greater than -1.4 V indicates hydrogen formation ($2H_2O+2e^- \rightarrow H_2+2OH^-$). The volume of hydrogen gas collected using electrodes CuO-30 min, CuO-60 min and CuO-1800 min at -1,8, 2 and 2.2 V in 1 M KOH is presented in Figure 10. At high coating times, the CuO electrode exhibits low catalytic performance for hydrogen evolution. This relatively high amount of H_2 generated on the CuO nanorod structure can be attributed that the morphology supply conductive channels for electron transport to improve hydrogen evolution and create hydrogen desorption sites [29]. The CuO-30 min electrode having nanorod morphology exhibits higher HER activity for all potentials indicated compared to other electrodes.

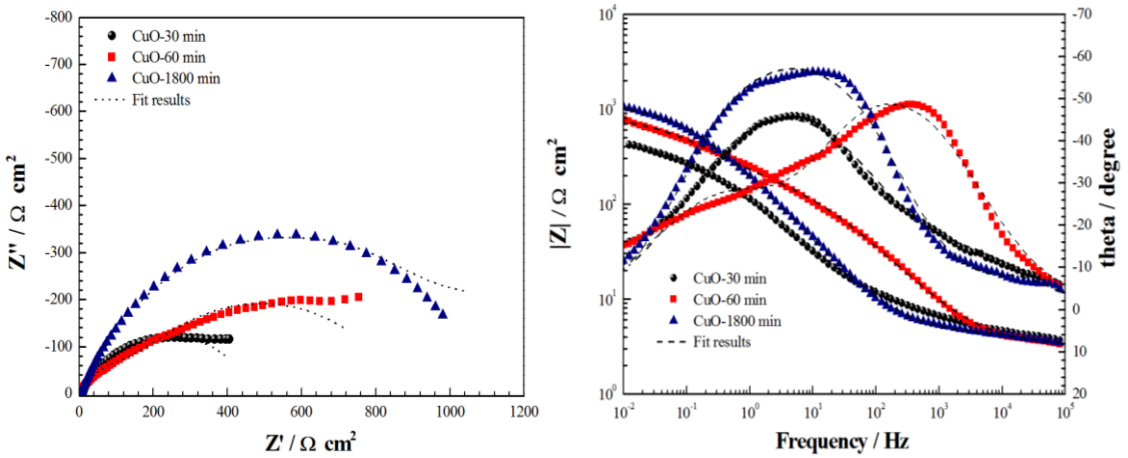

Figure 7. Electrochemical impedance results (Nyquist, Bode and phase angle plots) for CuO-30 min, CuO-60 min, and CuO-1800 min electrodes recorded at OCP in 1M KOH

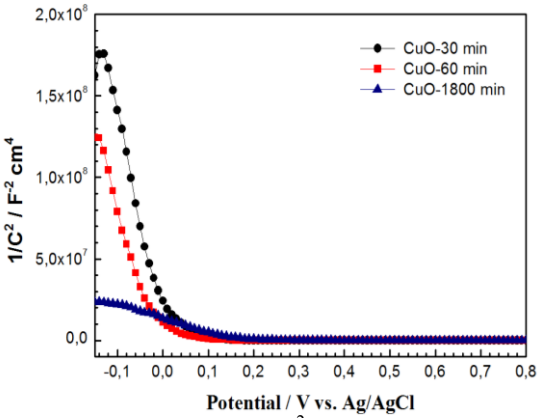

Figure 8. Variations of $1/C^2$ with applied potential (Mott-Schottky plot) for CuO-30 min, CuO-60 min and CuO-1800 min electrodes

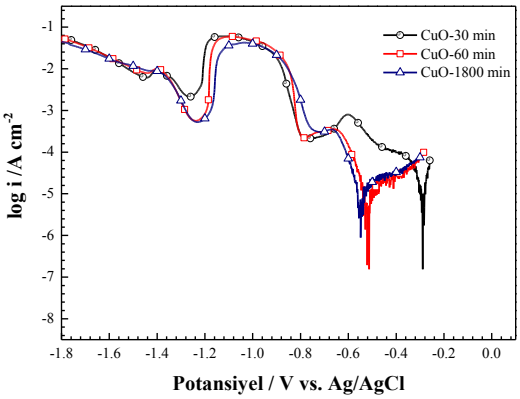

Figure 9. Cathodic polarization curves of for CuO-30 min, CuO-60 min and CuO-1800 min electrodes obtained in 1 M KOH solution at a scan rate of 0.01 Vs^{-1}

In literature, it was reported that hydrogen gas volumes produced on C/NiMn, C/NiMnZn, C/NiMnZn-PtRu and C/NiMnZn-PtPd electrodes by electrolysis technique applying 3.0 V over 1 h were in the range of 102-225 mL cm^{-2} [30]. In another study, it was stated that the hydrogen gas volumes formed by electrolysis in 1M KOH at a constant current density of 30 mA over 1 h for the C @ FeZn, C@FeZn/Pt, C@FeZn/Ru electrodes were the range of 54-85 mL cm^{-2} [31]. The hydrogen evolution amounts obtained for low cost CuO electrodes at low potentials and short time can be said to have good potential compared to these electrodes reported in the literature.

For CuO-30 min, CuO-60 min and CuO-1800 min electrodes, the energy requirement (Q) and energy efficiency (η_{HHV}) values of alkali electrolysis at 25, 50 and 100 mA cm^{-2} current densities were calculated with the following equations [29,32]:

$$Q = I.U.t \tag{5}$$

$$\eta_{HHV} = \frac{283.3kJ/mol}{U.I.t} \tag{6}$$

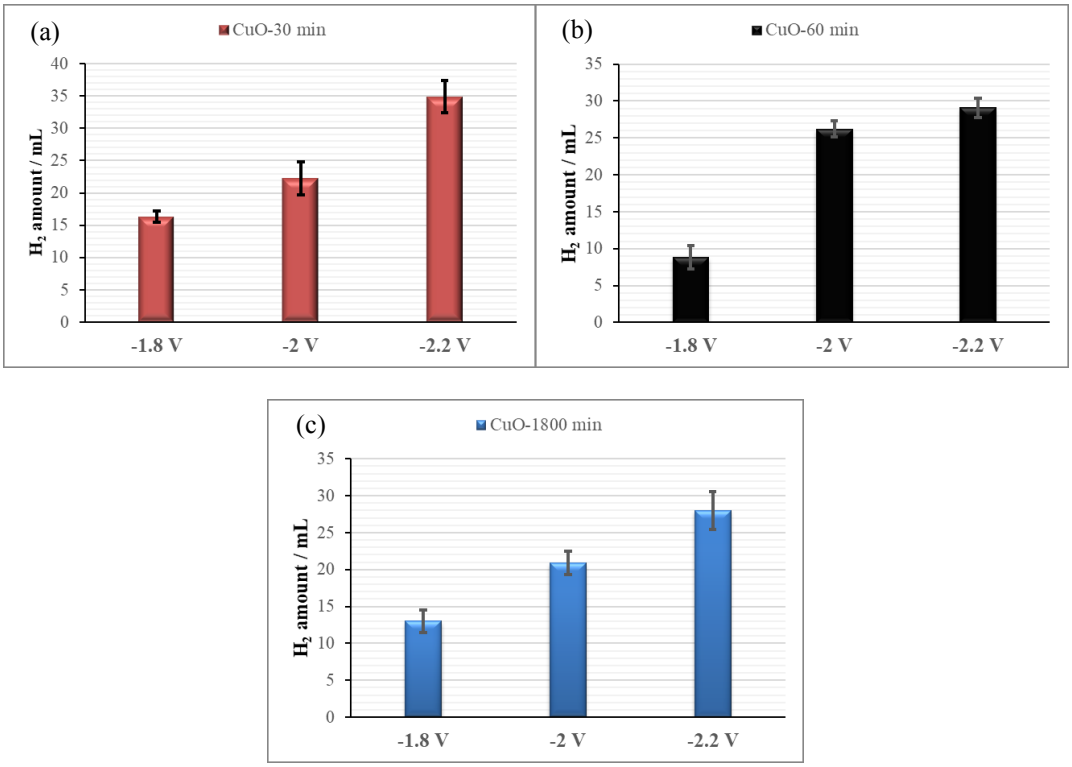

Figure 10. Hydrogen evolution amounts for CuO-30 min (a), CuO-60 min (b), and CuO-1800 min (c) electrodes in 1 M KOH solution at different cathodic potentials

Where I is the applied current in Ampere, U is the cell voltage in Voltage and t is time of evolution of a 1 mol of hydrogen in seconds. The results are given in Figure 11. When the values are compared at the current density of 100 mA/cm^2, the energy consumption is partially increased with increased coating time. When the energy efficiency was considered, the order of electrocatalytic activity of the studied CuO morphologies was determined as CuO nanorod> CuO nanoflakes> CuO nano-flower. When the results were examined, it was seen that the energy efficiency values of CuO

electrodes were very close to one. The best energy efficiency was found to belong to CuO nanorod morphology. Considering the electrochemical results of CuO electrodes, CuO-30 min electrode was determined as the ideal electrode.

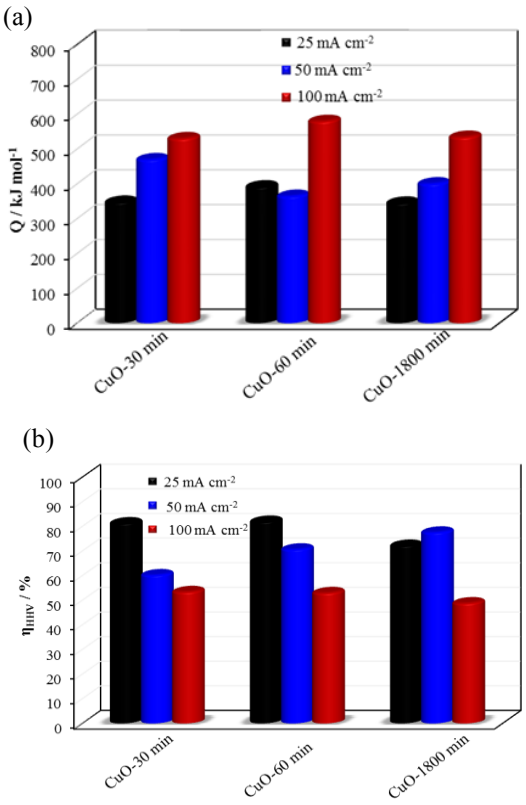

Figure 11. Energy consumption (a) and efficiency (b) of alkaline electrolysis at 25, 50, and 100 mA cm^{-2} current densities for for CuO-30 min, CuO-60 min, and CuO-1800 min electrodes

4. CONCLUSIONS

Hydrogen, which is regarded as a clean energy carrier, can be produced by many methods. Among these, hydrogen gas production by electrolysis of water is the most suitable. The most important problem limiting the applicability of this method is; It is the cost increase due to the overvoltages that occur in the system. To solve this problem, the appropriate electrode is being investigated.

In the work, CuO nanostructures were synthesized chemical techniques. To determine the appropriate production conditions for the HER reaction, CuO nanostructures were synthesized at the different times. The morphology and structure of CuO nanostructures electrodes were characterized in detail by FE-SEM, EDX, BET and XRD. The nanorod, nanoplate (nanoflakes) and nano-flower-like CuO structures were obtained. Cathodic polarization, impedance measurements and Mott-Schottky analysis were carried out. When the electrochemical results were examined, it was determined that CuO-30 min electrode produced more chemically was more effective than other morphologies.

5. ACKNOWLEDGMENTS

The authors are thankful to the Kilis 7 Aralık University research fund (Project number: MAP-11491) for their financial support.

6. REFERENCES

1. Sun, Y., Yan, K.P., 2014. Effect of Anodization Voltage on Performance of TiO_2 Nanotube Arrays for Hydrogen Generation in a Two-compartment Photoelectrochemical Cell, International Journal of Hydrogen Energy 39(22), 11368-11375.

2. Wang, J.X., Huang, J., Xie, H.L., Qu, A.L., 2014. Synthesis of g-C3N4/TiO2 With Enhanced Photocatalytic Activity for H-2 Evolution by a Simple Method, International Journal of Hydrogen Energy 39(12), 6354-6363.

3. Guo, S.Y., Zhao, T.J., Jin, Z.Q., Wan, X.M., Wang, P.G., Shang, J., Han, S., 2015. Self-Assembly Synthesis of Precious-metal-free 3D ZnO Nano/micro Spheres With Excellent Photocatalytic Hydrogen Production from Solar Water Splitting, Journal of Power Sources 293, 17-22.

4. Zhou, H., Pan, J.Y., Ding, L., Tang, Y.W., Ding, J., Guo, Q.X., Fan, T., Zhang, D., 2014. Biomass-derived Hierarchical Porous CdS/M/TiO2 (M = Au, Ag, pt, pd) Ternary Heterojunctions for Photocatalytic Hydrogen

Evolution, International Journal of Hydrogen Energy 39(29), 16293-16301.

5. Cui, X.F., Jiang, G.Y., Zhu, M., Zhao, Z., Du, L.C., Weng, Y.X., Xu, C., Zhang, D., Zhang, Q., Wei, Y., Duan, A., Liu, J., Gao, J., 2013. TiO_2/CdS Composite Hollow Spheres With Controlled Synthesis of Platinum on the Internal Wall for the Efficient Hydrogen Evolution, International Journal of Hydrogen Energy 38(22), 9065-9073.

6. Harun, N.F.A.B., bin Mohd, Y., Pei, L.Y., Chin, L.Y., 2018. Fabrication of Tungsten Trioxide-loaded Titania Nanotubes as a Potential Photoanode for Photoelectrochemical Cell, International Journal of Electrochemical Science 13(5), 5041-5053.

7. Townsend, T.K., Sabio, E.M., Browning, N.D., Osterloh, F.E., 2011. Photocatalytic Water Oxidation with Suspended Alpha-Fe_2O_3 Particles-effects of Nanoscaling, Energy & Environmental Science 4(10), 4270-4275.

8. Berglund, S.P., Flaherty, D.W., Hahn, N.T., Bard, A.J., Mullins, C.B., 2011. Photoelectrochemical Oxidation of Water Using Nanostructured BiVO4 Films, Journal of Physical Chemistry, C 115(9), 3794-3802.

9. Wu, Q.Y., Diao, P., Sun, J., Xu, D., Jin, T., Xiang, M., 2015. Draining the Photoinduced Electrons Away from an Anode: the Preparation of Ag/Ag_3PO_4 Composite Nanoplate Photoanodes for Highly Efficient Water Splitting, Journal of Materials Chemistry A 3(37), 18991-18999.

10. Chen, Z.B., Jaramillo, T.F., Deutsch, T.G., Kleiman-Shwarsctein, A., Forman, A.J., Gaillard, N., Takanabe, K., Heske, C., Sunkara, M.K, McFarland, E.W., Domen, K., Miller, E., Turner, J.A., Dinh, H.N., 2010. Accelerating Materials Development for Photoelectrochemical Hydrogen Production: Standards for Methods, Definitions, and Reporting Protocols, Journal of Materials Research 25(1), 3-16.

11. Khaselev, O., Turner, J.A., 1998. A Monolithic Photovoltaic-photoelectrochemical Device for Hydrogen Production Via Water Splitting, Science 280(5362), 425-427.

12. Gao, L., Cui, Y.C., Wang, J., Cavalli, A., Standing, A., Vu, T., Verheijen, M.A., Haverkort, J.E.M., Bakkers, E., Notten, P.H.L., 2014. Photoelectrochemical Hydrogen Production on InP Nanowire Arrays with Molybdenum Sulfide Electrocatalysts, Nano Letters 14(7), 3715-3719.

13. McKone, J.R., Pieterick, A.P., Gray, H.B., Lewis, N.S., 2013. Hydrogen Evolution from Pt/Ru-Coated p-Type WSe_2 Photocathodes, Journal of the American Chemical Society 135(1), 223-231.

14. Dominey, R.N., Lewis, N.S., Bruce, J.A., Bookbinder, D.C., Wrighton, M.S., 1982. Improvement of Photo-Electrochemical Hydrogen Generation by Surface Modification of P-Type Silicon Semiconductor Photo-Cathodes, Journal of the American Chemical Society 104(2), 467-482.

15. Huang, Q., Li, Q., Xiao, X.D., 2014. Hydrogen Evolution from Pt Nanoparticles Covered p-Type CdS:Cu Photocathode in Scavenger-Free Electrolyte, Journal of Physical Chemistry C 118(5), 2306-2311.

16. Nancheva, N., Docheva, P., Misheva, M., 1999. Defects in Cu and Cu-O Films Produced by Reactive Magnetron Sputtering, Materials Letters 39(2), 81-85.

17. Mu, C., He, J.H., 2011. Confined Conversion of CuS Nanowires to CuO Nanotubes by Annealing-induced Diffusion in Nanochannels, Nanoscale Research Letters 6.

18. Shen, X.P., Liu, H.J., Pan, L., Chen, K.M., Hong, J.M., Xu, Z., 2004. An Efficient Template Pathway to Synthesis of Ordered Metal Oxide Nanotube Arrays using Metal Acetylacetonates as Single-source Molecular Precursors, Chemistry Letters 33(9), 1128-1129.

19. Chaudhary, A., Barshilia, H.C., 2011. Nanometric Multiscale Rough CuO/Cu(OH)(2) Superhydrophobic Surfaces Prepared by a Facile One-Step Solution-Immersion Process: Transition to Superhydrophilicity with Oxygen Plasma Treatment, Journal of Physical Chemistry C 115(37), 18213-18220.

20. Schlur, L., Bonnot, K., Spitzer, D., 2014. Synthesis of Cu(OH)(2) and CuO Nanotubes Arrays on a Silicon Wafer, Rsc Advances 5(8), 6061-6070.

21. Ke, X., Zhou, X., Gao, H., Hao, G.Z., Xiao, L., Chen, T., Liu, J., Jiang, W., 2018. Surface Functionalized Core/shell Structured CuO/Al Nanothermite with Long-term Storage Stability and Steady Combustion Performance, Materials & Design 140(15), 179-187.

22. Zhang, Q.B., Zhang, K.L., Xu, D.G., Yang, G.C., Huang, H., Nie, F.D., Liu, C., Yang, S., 2014. CuO Nanostructures: Synthesis, Characterization, Growth Mechanisms, Fundamental Properties, and Applications, Progress in Materials Science 60(1), 208-337.

23. Guo, X., Diao, P., Xu, D., Huang, S., Yang, Y., Jin, T., Wu, Q., Xiang, M., Zhang, M., 2014. CuO/Pd Composite Photocathodes for Photoelectrochemical Hydrogen Evolution Reaction, International Journal of Hydrogen Energy 39(15), 7686-7696.

24. Li, Z.Z., Xin, Y.M., Zhang, Z.H., Wu, H.J., Wang, P., 2015. Rational Design of Binder-free Noble Metal/metal Oxide Arrays with Nanocauliflower Structure for Wide Linear Range Nonenzymatic Glucose Detection, Scientific Reports 5, 10617.

25. Espejo, E.M.A., Balela, M.D.L., 2017. Facile Synthesis of Cupric Hydroxide and Cupric Oxide on Copper Foil for Potential Electrochemical Applications, 7th International Conference on Key Engineering Materials (Ickem 2017) 201.

26. Amin, M.A., Fadlallah, S.A., Alosaimi, G.S., 2014. In Situ Aqueous Synthesis of Silver Nanoparticles Supported on Titanium as Active Electrocatalyst for the Hydrogen Evolution Reaction, International Journal of Hydrogen Energy 39(34), 19519-19540.

27. Mahmood, A., Tezcan, F., Kardas, G., 2017. Photoelectrochemical Characteristics of CuO Films with Different Electrodeposition Time, International Journal of Hydrogen Energy 42(36), 23268-23275.

28. Hao, X.Q., Wang, Y.C., Zhou, J., Cui, Z.W., Wang, Y., Zou, Z.G., 2018. Zinc Vacancy-promoted Photocatalytic Activity and Photostability of ZnS for Efficient Visible-light-driven Hydrogen Evolution, Applied Catalysis B-Environmental 221, 302-311.

29. Herraiz-Cardona, I., Ortega, E., Vazquez-Gomez, L., Perez-Herranz, V., 2011. Electrochemical Characterization of a NiCo/Zn Cathode for Hydrogen Generation, International Journal of Hydrogen Energy 36(18), 11578-11587.

30. Yuce, A.O., Doner, A., Kardas, G., 2013. NiMn Composite Electrodes as Cathode Material for Hydrogen Evolution Reaction in Alkaline Solution, International Journal of Hydrogen Energy 38(11), 4466-4473.

31. Farsak, M., Telli, E., Yuce, A.O., Kardas, G., 2017. The Noble Metal Loading Binary Iron-zinc Electrode for Hydrogen Production, International Journal of Hydrogen Energy 42(10), 6455-6461.

32. Nikolic, V.M., Tasic, G.S., Maksic, A.D., Saponjic, D.P., Miulovic, S.M., Kaninski, M.P.M., 2010. Raising Efficiency of Hydrogen Generation from Alkaline Water Electrolysis-Energy Saving, International Journal of Hydrogen Energy 35(22), 12369-12373.